Proceedings of IMECE:
2000 International Mechanical Engineering Congress and Exhibit
November 5-10, 2000, Orlando, FL

ASME HTD 2-8-2

HEAT TRANSFER IMPLICATIONS IN THE FIRST MEMS FABRICATED THERMAL TRANSPIRATION-DRIVEN VACUUM PUMP FOR GASES

Stephen E. Vargo and Amanda A. Green
Jet Propulsion Laboratory, California Institute of Technology, M/S 302-231
4800 Oak Grove Dr., Pasadena, CA 91109
(818) 354-2824, (818) 393-4540 fax
email: Stephen.E.Vargo@jpl.nasa.gov

E. P. Muntz
Dept. of Aerospace and Mechanical Eng.
University of Southern California
Los Angeles, CA 90089

ABSTRACT

The success of NASA's future space missions and the development of portable, commercial instrument packages will depend greatly on miniaturized components enabled by the use of microelectromechanical systems (MEMS). Both of these application markets for miniaturized instruments are governed by the use of MEMS components that satisfy stringent power, mass, volume, contamination and integration requirements. An attractive MEMS vacuum pump for instruments requiring vacuum conditions is the Knudsen Compressor, which operates based on the rarefied gas dynamics phenomenon of thermal transpiration. Thermal transpiration describes the regime where gas flows can be induced in a system by maintaining temperature differences across porous materials under rarefied conditions. This pumping mechanism provides two overwhelmingly attractive features as a miniature vacuum pump - no moving parts and no working fluids or lubricants. Due to favorable power, volume and mass estimates a Knudsen Compressor fabricated using MEMS fabrication techniques (lithography, deep reactive ion etching) and new materials (silicon, aerogel) has been completed. The experimental testing of this MEMS Knudsen Compressor device's thermal and pumping performance are outlined in this manuscript. Good agreement between experiments and numerical predictions using a transitional flow analysis have also been obtained although simple simulations based on the aerogel's structure are difficult to perform.

NOMENCLATURE

A_{cd}	surface area of a material normal to the heat flow
A_{cv}	surface area of a material for convection
A_r	surface area of a material for radiation
h	heat transfer coefficient for convection
K_m	thermal conductivity of a material
Kn	Knudsen number in the region of interest
L	characteristic system dimension or material thickness
L_r	tube radius
p	pressure in the region of interest
Q_P	Poiseuille flow coefficient
Q_T	thermal transpiration flow coefficient
$\dot{Q}_{cd}$	heat transfer due to conduction
$\dot{Q}_{cv}$	heat transfer due to convection
$\dot{Q}_r$	heat transfer due to radiation
$\dot{Q}_T$	total heat transfer
T	temperature in the region of interest
$(\Delta p_I)_T$	maximum pressure difference in a stage
ΔT	temperature difference in a region of interest
ε	emissivity of a material
λ	mean free path of the working gas
σ	Stefan-Boltzmann constant

INTRODUCTION

Due to recent budgetary concerns the National Aeronautics and Space Administration (NASA) has adopted a smaller, more frequent and focused mission approach for their robotic exploration programs. The success of these missions will undoubtedly rely on the advantages MEMS provide, such as smaller resultant system mass, volume and power consumption values. The benefits miniaturization enables has led to a great deal of governmental as well as commercial interest in the development of portable, integrated analytical instruments. Mass spectrometers, optical spectrometers, gas chromatographs, electron beam optics and on-demand gas generators are some of the devices in various stages of MEMS development. Existing and planned analytical instrument packages at the Jet Propulsion Laboratory (JPL) lack unique and integrated methods towards satisfying their vacuum needs for an array of *in situ* sampling and analyzing missions currently under study. It is well known that the currently available commercial rough vacuum pumps cannot meet the requirements imposed by the miniaturized analytical instruments proposed for portable use. Commercial pumps are greatly oversized for the small flows needed and pose serious technical challenges towards their miniaturization. In these small instrument systems the vacuum

pump tends to have the greatest mass, volume, power consumption and cost penalties. Obviously, miniaturized and possibly integrated vacuum pumps would greatly increase the attractiveness of these types of instruments. The few number of existing miniaturized vacuum pumps, suffer from either negative scaling issues, poor performance, constraining operation or detrimental system impacts. Based on these issues and future NASA mission requirements it is clear that successful MEMS vacuum pumps cannot be simply scaled-down versions of commercially available pumps. The Knudsen Compressor, which was originated at the University of Southern California (USC) in 1993 and is currently in joint development with JPL, is an attractive vacuum pump that can provide pumping of gases in the pressure range of 1 mTorr (possibly down to 0.1 mTorr) to 760 Torr.

Knudsen Compressors have two overwhelmingly attractive features as miniaturized vacuum pumps - no moving parts and no fluids or lubricants. These pumps are driven by the rarefied gas dynamics phenomenon of thermal transpiration. The results of thermal transpiration may be illustrated by considering a system consisting of two volumes of gas connected by a tube whose radius (L_r) is small compared to the mean free path of the gas (λ). In this case the system flow regime is considered to be free molecular where system interactions are dominated by gas-surface collisions and gas-gas collisions can be neglected. Based on the local Knudsen number (Kn), which is the ratio of the mean free path of the gas to a characteristic system dimension (L) (i.e. $Kn = \lambda/L$), a given location can exhibit continuum $Kn \le 0.01$, transitional $0.01 < Kn < 10$ or free molecular $Kn \ge 10$ flow behavior. If the two volumes are maintained at temperatures T_1 and T_2, but are otherwise undisturbed, the equilibrium pressures p_1 and p_2 of the two volumes are related by $p_1/p_2 = \sqrt{T_1/T_2}$. In many instances thermal transpiration tends to be a laboratory curiosity at normal dimensions and correspondingly low pressures. However, in the micromechanical domain it can form the basis for important systems because free molecular conditions can exist at much higher pressures due to the characteristically smaller dimensions of MEMS structures. The recent availability of nanopore materials with low thermal conductivity and MEMS fabrication techniques have significantly expanded the utilization of thermal transpiration as a pumping mechanism. These developments allow the construction of a thermal transpiration-driven vacuum pump that can operate under free molecular conditions over a wider and more useful pressure range (from about 1 mTorr to above 760 Torr). Through proper materials selection and pump design the Knudsen Compressor aims to utilize this phenomenon in order to create functional MEMS vacuum pumps.

ANALYSIS OF A SINGLE STAGE THERMAL TRANSPIRATION VACUUM PUMP

The single stage analysis presented here is a summary of a detailed analysis presented by Vargo *et al.* [1] for multiple staged Knudsen Compressor operation. Knudsen Compressors generate large changes in pressure for most systems by utilizing a cascade of multiple, individually heated stages. A schematic of one stage is shown in Fig. 1, where each stage in the pump consists of a capillary and connector section. A temperature increase across the capillaries results in a thermal transpiration driven pressure increase. The capillary section is followed by a connector section where the pressure is approximately constant while the temperature drops to its original value prior to entering the next stage.

The maximum pressure difference (i.e. no mass flow for steady state conditions) between the hot and cold sides of a single stage Knudsen Compressor is

$$(\Delta p_I)_T = \frac{p_{AVG}\Delta T}{T_{AVG}}\left[\frac{Q_T}{Q_P} - \frac{Q_{T,C}}{Q_{P,C}}\right] \tag{1}$$

where p_{AVG}, ΔT and T_{AVG} are the average pressure, temperature difference across the transpiration membrane and the average temperature, respectively. Q_T and Q_P are the thermal transpiration and Poiseuille flow coefficients for cylindrical tubes, respectively. These flow coefficients have been numerically determined and are functions of Kn. The subscript C refers to the connector section of the stage and the flow coefficients without subscript refer to the capillary section. The ratio Q_T/Q_P varies from close to 0.5 near free molecular conditions to $6\text{x}10^{-3}$ near continuum conditions. It is evident that the operation of the Knudsen Compressor will change dramatically in the transitional flow regime. The average pressure in the stage is identically equal to

$$p_{AVG} = p_0 + \frac{(\Delta p_I)_T}{2} \tag{2}$$

with p_0 the inlet pressure to the stage (i.e. the cold side pressure).

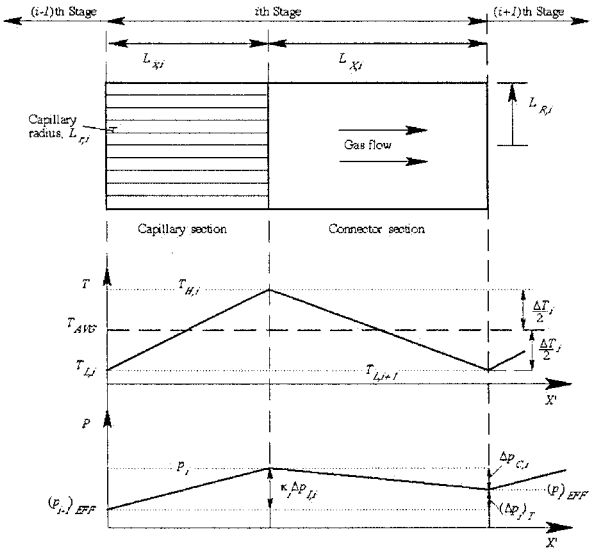

Figure 1: Illustrative *i*th stage of a Knudsen Compressor.

SINGLE STAGE MEMS KNUDSEN COMPRESSORS

Device Design and Fabrication

The MEMS devices that have been fabricated (see Figs. 2 and 3) consist of two silicon chips (thermal guards), which are each 2.025 cm x 2.025 cm and 400 μm thick, an aerogel membrane (520 μm thick), two Corning Pyrex® 7740 plenums and two aluminum vacuum connectors. The silicon chips (a hot side and cold side) and the aerogel, which is a porous membrane made of suspended SiO_2 particles, serve as the improved thermal guards and transpiration membrane in comparison to the proof-of-concept Knudsen Compressors [2,3], respectively. Each silicon chip has

been deep reactive ion etched (DRIE) with a dense array of 20 μm diameter holes through the chip's thickness (i.e. cylindrical tubes) for gas passage. A thin gold film heater is also patterned on each silicon chip for the establishment of device temperatures warmer than ambient. The heater acts a resistive path to an applied current and resistively heats to a desired hot temperature needed for stage operation. The aerogel has an average pore size of 20 nm and a very low thermal conductivity (17 mW/mK at 760 Torr) providing the essential requirements for thermal transpiration to result when a voltage is applied to one of the heaters. In normal operation, the cold side is not actively cooled and remains cooler than the hot side due to the sandwiched aerogel membrane. A thin perimeter bead of Torr Seal® epoxy is used to secure the thermal guards and aerogel together. Pyrex plenums are anodically bonded to the silicon chips and serve as mating pieces to two machined aluminum vacuum connectors.

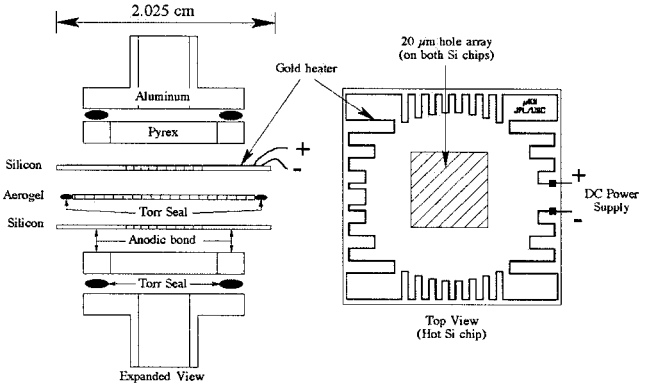

Figure 2: Schematic of the single stage MEMS Knudsen Compressor.

Vacuum tubing is attached to the machined aluminum pieces to connect the device to pumping and gas input lines. Gas pumping in the device is made possible by establishing a temperature gradient across the aerogel membrane using the hot side's heater. The performance of this design using new materials and fabrication techniques is critical to the realization of a Knudsen Compressor cascade composed of many individually operated stages. The MEMS Knudsen Compressor shown in Fig. 3 is fabricated using MEMS fabrication techniques and silicon, aerogel, Pyrex and aluminum parts. Selected mechanical and thermal properties of these materials are included for reference in Table 1. The following discussion outlines the necessary MEMS device fabrication steps.

MEMS Processing of the Thermal Guards.

The role of the thermal guards is to provide a mechanism by which incoming molecules have their temperature adjusted to desired values before they pass through the transpiration membrane. This ensures that those molecules striking and passing through the thermal guard structure towards the transpiration membrane have first accommodated to a desired temperature. The temperature gradient across the faces of the transpiration membrane is the only gradient creating the thermal transpiration-driven gas flow. Accurate temperature readings at the membrane faces are difficult to obtain unobtrusively in these devices so readings on the outside of the device are performed using small thermocouples. Utilizing a thermal guard material of high thermal conductivity helps to minimize the gradient that may exist across the thermal guard during operation and results in a uniform temperature throughout the guard. Silicon is chosen as the material of the thermal guard in the MEMS device since it has a high thermal conductivity (150 W/mK) and can be machined to a desired structure using MEMS processing procedures and equipment available in the Microdevices Laboratory at JPL. An etched silicon thermal guard that has a 20 μm diameter hole array with 10 μm spacing between holes is shown in Fig. 4. This scanning electron micrograph (SEM) of the thermal guard, which was cleaved (i.e. broken along one of the crystallographic planes using a metal scribe) in the middle of the hole array, shows the unique etch capabilities enabled through the use of the DRIE system.

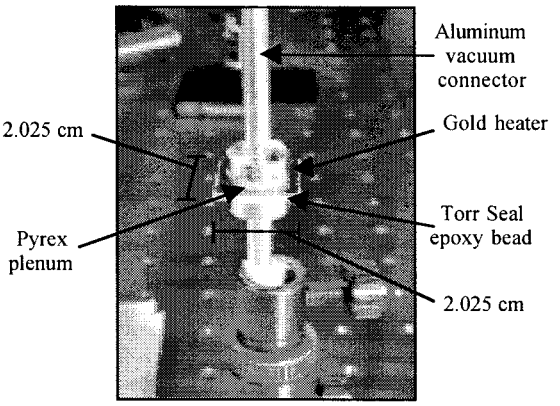

Figure 3: Fabricated single stage MEMS Knudsen Compressor.

Table 1: Selected material properties of the single stage MEMS Knudsen Compressor components.

Material	Thermal Conductivity, W/mK	Density, g/cm^3	Thermal Expansion, 1x10^{-6}/K	Max. Use Temp., K
Si	150	2.33	4.2	1685
Aerogel	0.017	0.1	3.0	773
Pyrex 7740	1.13	2.23	3.25	763
Torr Seal	0.435	1.6	30.3	423
Al 6061	180	2.70	23.6	890

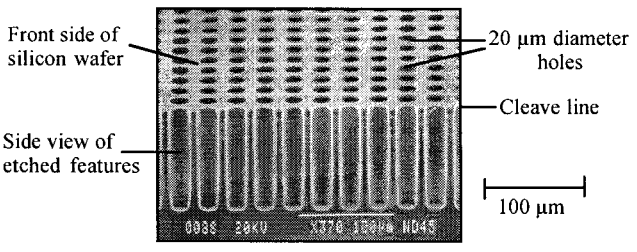

Figure 4: SEM of the thermal guard hole array structure enabled through the use of DRIE.

The DRIE system used for the thermal guard fabrication is an ICP RIE manufactured by Surface Technology Systems (STS) and is available in the Microdevices Laboratory. Silicon wafers are

patterned with photoresist layers in order to selectively etch desired features. The hole arrays that have been tested consist of 20 μm diameter holes spaced by 40 μm in a central 0.5 cm^2 area per thermal guard (see Fig. 2). The silicon etch process for the thermal guards is outlined in Fig. 5 with the batch fabrication methods of MEMS processing allowing about $1.4x10^4$ holes to be fabricated simultaneously in each thermal guard (8.75% open area in the array) with 8 thermal guards being fabricated in each 100 mm diameter, 400 μm thick silicon wafer. The DRIE process is the only technique currently available that can provide the high aspect ratio, high feature density and through wafer etching capabilities required in this project. A front and back side etch using the STS DRIE creates the 20 μm diameter hole array through the silicon wafers. Back side alignment using wafer and mask alignment marks allows the front and back side features to meet within ± 2 μm.

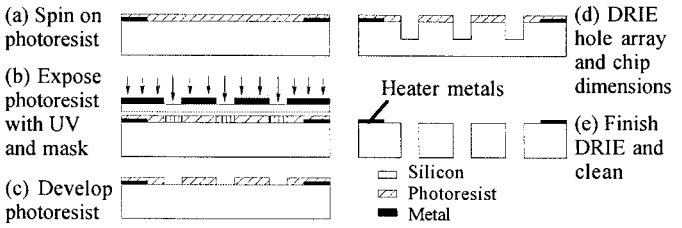

Figure 5: Processing steps for the DRIE of the thermal guards.

The first etch is completed at a depth of 200 μm and the wafer is subsequently cleaned of photoresist. A photoresist layer is deposited on the back side of the wafer for patterning. A back side alignment using the alignment marks on the wafer's front side with those of the etch mask ensure proper alignment. The wafer is then placed on a carrier wafer (photoresist side up) and secured with wax to ensure that the STS chuck is not damaged upon etching through the device wafer. After a total of 210 minutes of etching (etch rate < 2.5 μm/min) the individual thermal guards have been machined. A thorough cleaning removes residual photoresist and wax from the devices. A check of the hole array alignment can be made by cleaving one of the unused thermal guards along its hole array. Fig. 6 shows a typical alignment possible (this alignment is about ± 1 μm) using back side alignment on the mask aligner. The jagged features shown in this SEM are partial silicon tubes that remained after cleaving. Cleaving does not provide much control over where the silicon breaks.

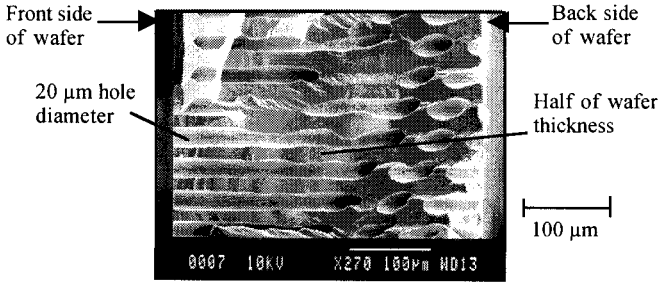

Figure 6: Alignment check for the etched thermal guard hole array.

Aerogel as a Thermal Transpiration Membrane.

Thermal transpiration over useful pressure ranges in a Knudsen Compressor requires the use of a material that has both low thermal conductivity and small internal pores. The use of an aerogel membrane enables the construction of a MEMS version of the Knudsen Compressor. Aerogels are a special class of continuously porous solid materials which are characterized by nanometer size particles and pores. These materials have an average composition of only 5% solid material (SiO_2) and 95% open space leading to the commonly referred name "frozen smoke." This rather empty structure (see Fig. 7) results in a thermal conductivity that varies with the ambient pressure (17 mW/mK at 760 Torr and 8 mW/mK at $p < 1$ Torr) [4]. Particles of diameters 2-5 nm and pores of diameters 10-100 nm, produce a solid-gas matrix in which the volume fraction of the solid can be less than 5%. The pore size distribution for aerogels, which make direct numerical simulations difficult, can be obtained by nitrogen adsorption/condensation analysis [5]. In the MEMS Knudsen Compressor a plain silica based aerogel has been used and its thickness and mean pore size are 520 μm and 20 nm, respectively. This pore size provides free molecular conditions at atmospheric pressure ($Kn = 6.4$ for air at 760 Torr).

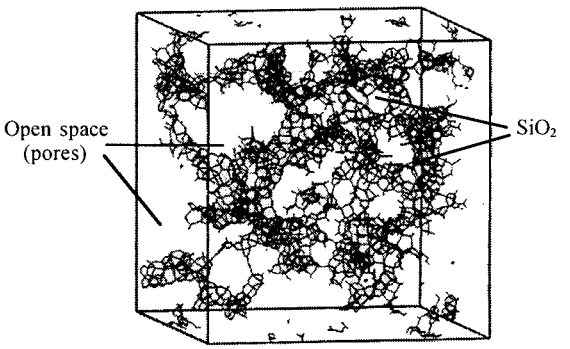

Figure 7: Schematic description of aerogel's structure [5].

Vacuum Connectors.

Pyrex 7740 and aluminum 6061 have been conventionally machined in order to make MEMS device vacuum connectors. Each Pyrex piece, which is a glass ring with an inner diameter of 1 cm, an outer diameter of 1.5 cm and thickness of 2 mm, is anodically bonded to the silicon and acts as a gas plenum. The aluminum connectors, which have similar dimensions and shape to the Pyrex plenum on one end and a straight 4.5 cm length of 0.635 cm diameter tubing on the other end, are then bonded to the Pyrex plenums using Torr Seal epoxy. Cajon® Ultra Torr o-ring sealing vacuum connectors are then attached to the aluminum tube ends in order to attach vacuum and gas input lines.

Assembly and Bonding.

Vacuum tight sealing of the various Knudsen Compressor components is imperative to determining actual device performance under experimental conditions. The small pressures differences generated (< 20 Torr) across a single stage dictate that the experimental device and system be leak tight. Even small leaks are intolerable since they cannot be distinguished from the thermal transpiration pressure increases simply. Anodic bonding of the Pyrex plenums to the silicon thermal guards ensures the required

vacuum tight seal. A thin bead of Torr Seal epoxy around the perimeter of the thermal guard and aerogel membrane sandwich was found to be the best method of forming this seal. An additional epoxy bond between each Pyrex plenum and aluminum vacuum connector provide the final vacuum seals.

The epoxy bond between the thermal guards and the aerogel membrane is the bond of interest in the MEMS devices. Two identically fabricated single stage devices, which are referred to as μKn1 (first version) and μKn2 (second version), were epoxy bonded near the aerogel slightly different in order to investigate the impact this epoxy would have on device performance (see Fig. 8). The first version was assembled using two separate beads of epoxy to validate the epoxy as a viable sealing approach and to ensure that the device was leak tight. The second device used a wider aerogel membrane that was the same dimensions as the thermal guard chips and only had an epoxy bead around the perimeter of the device thickness. This is done in order to minimize the heat conduction path between the hot and cold thermal guards since Torr Seal has a much higher thermal conductivity than aerogel (about 26 times greater). These bonding approaches result in different device heat transfer, which correspond to different performance, due to the location and amount of epoxy used. Less heat transfer for the same input heater power was seen for μKn2 in comparison to μKn1. The experimental results for both devices are discussed in the following section.

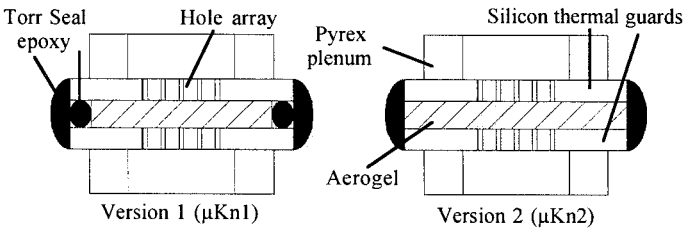

Figure 8: Different epoxy bond approaches for the two single stage MEMS devices.

RESULTS AND DISCUSSION

Experimental Layout

The experimental setup for the single stage MEMS Knudsen Compressor devices is shown in Fig. 9. Each device is connected to the rest of the vacuum system using lengths of Polyflo® plastic and stainless steel tubing. The tubing is connected to each other and to other components using an assortment of Swagelok® vacuum fittings. This system is pumped out to low pressures using a mechanical pump (blank-off pressure of 5 mTorr) which is able to provide an ultimate pressure of about 230 mTorr when either MEMS device is included in the system. Working gases, which were Ar, CO_2, He and N_2, from regulated, high-pressure gas bottles are introduced into the system using plastic tubing and in-line filters. The thermal transpiration efficiency will depend on the actual working gas. Helium remains more rarefied than does CO_2 at the same pressure and hence leads to better performance. Absolute pressures in the system are measured using a 10 Torr and 1000 Torr MKS Instruments Baratron® absolute pressure transducers (type 122). Pressure differences between the output (hot side) and input (cold side) of the devices are measured using a 10 Torr Baratron® differential pressure transducer (type 223). Temperatures on the silicon thermal guards are found using small, accurately placed thermocouples which have their measurements displayed using Omega CN310 temperature controllers. Power is supplied to each MEMS device's heater using a DC power supply (0-60 V, 0-1 A), BNC cables and a pair of micropositioner probes. Each probe allows the accurate placement of a thin (12 μm diameter) tungsten tip to one end of the heater. These probes provide electrical contact between the power supply output and input BNC cables and the thin-film heater. Two digital Fluke 87 III multimeters are also connected in the system in order to measure the voltage drop across the heater and the current through the heater (see Fig. 9). During device heating these measurements are used to calculate the operational power required for measured device temperatures. In order to investigate the usefulness of the fabricated MEMS single stage devices and their corresponding maximum pressure differentials $\left((\Delta p_I)_T\right)$, heat transfer and throughput experiments were conducted.

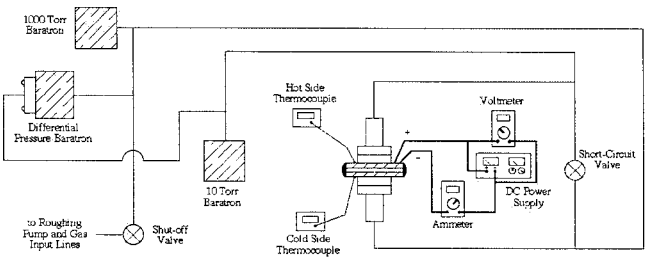

Figure 9: Experimental layout of the MEMS single stage devices.

Constant System Pressure Experiments

Maximum pressure differential measurements $\left((\Delta p_I)_T\right)$ at varying heater temperatures have been made for both MEMS single stage devices under a constant system pressure of 760 Torr using Ar, CO_2, He and N_2 working gases. These $(\Delta p_I)_T$ values, which are measured using the differential Baratron transducer, are made by closing the short-circuit valve and noting the maximum attainable pressure difference between the two sides of the devices. The short-circuit is closed only when an established temperature has been reached for any given heater power input (see Fig. 9). In order to investigate the performance of each device for a given working gas the input power to the heaters was increased by increasing the voltage from the DC power supply. Increases in the voltage drop across the heater result in increased hot side temperatures. Higher temperatures generally result in larger $(\Delta p_I)_T$ values at the same pressure. Figure 10 shows the results for both single stage devices when operated on helium and nitrogen. Note that the $(\Delta p_I)_T$ values have been normalized by the inlet system pressure (p_0), which is the pressure measured on the cold side of the device, in order to properly compare the results from each device.

As expected, helium has a much better performance for the same input power in each device. It is interesting to note that the μKn2 device has significantly better performance than the μKn1 device. At a device input power of 1.5 W, the $(\Delta p_I)_T$ values at p_0 = 760 Torr for the helium μKn1, helium μKn2, nitrogen μKn1 and nitrogen μKn2 cases are 5.08 Torr, 9.54 Torr, 3.39 Torr and 5.09 Torr, respectively. The helium μKn2 data is 1.88 times higher than the helium μKn1 data and the nitrogen μKn2 data is 1.5 times

higher than the nitrogen μKn1 data at this heater power. These factors become larger as the heater power is increased. These differences between the two devices can be attributed to their slightly different epoxy sealing approaches (see Fig. 8).

Since the second MEMS device (μKn2) appears to function better for the same operational inputs it is important to discuss the impact working gas has on device performance. The $(\Delta p_I)_T$ values for Ar, CO_2, He and N_2 for the μKn2 device are included in Fig. 11. At a heater input power of about 1.7 W the resultant $(\Delta p_I)_T$ for helium and carbon dioxide are about 11.5 Torr and 4.3 Torr, respectively. This is roughly a factor of 2.7 times better when operating on helium instead of carbon dioxide.

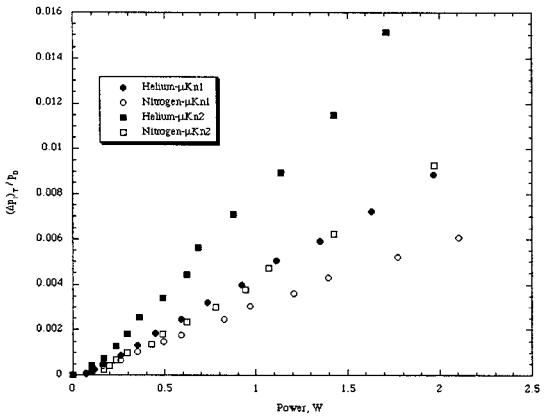

Figure 10: Differential pressure results for both MEMS devices for 760 Torr operation on He and N_2 with varying heater power.

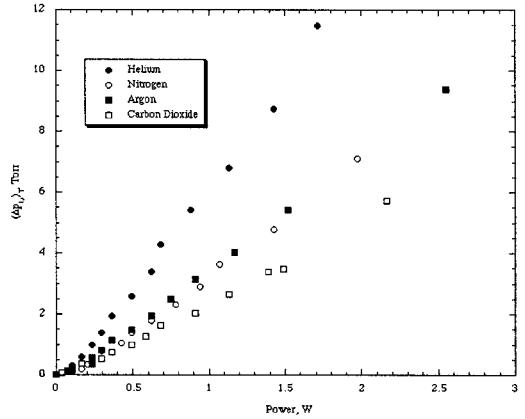

Figure 11: Differential pressures obtained with μKn2 at 760 Torr operation and various working gases.

Heat Transfer Estimates

In order to validate the power consumption values measured in the single stage devices for a given heater power, estimates of the device's heat transfer are essential. The constant heater power experiments presented in the previous section can be used for these estimates. Several temperatures, which have been measured at various locations on the μKn2 device, are used for a given applied heater power in order to estimate the energy losses. A temperature distribution in the μKn2 device has been measured for a constant power condition of 0.89 W at 760 Torr operation. This condition resulted in device hot and cold side temperature measurements of 305.5 K and 303 K, respectively.

The total heat transfer $\dot{Q}_T$ in each MEMS device is a sum of several heat conduction, convection and radiation terms [6]. The heat transfer due to conduction is

$$\dot{Q}_{cd} = \frac{K_m A_{cd} |\Delta T|_{cd}}{L} \tag{3}$$

where K_m, A_{cd}, $|\Delta T|_{cd}$ and L are the material's thermal conductivity, surface area normal to the heat flow, temperature gradient across and thickness, respectively. Conduction heat transfer in the single-stage devices is mainly from energy losses through the aerogel membrane, Torr Seal and Pyrex plenums (see Fig. 8). The estimated conduction values for the aerogel membrane (ΔT = 1.95 K, found from using Eq. (1) and the experimental conditions for the 0.89 W heater input power case), Torr Seal (ΔT = 2.5 K), Pyrex plenums (hot side ΔT = 1.5 K and cold side ΔT = 3 K) are 26.1 mW, 80.1 mW, 83.3 mW and 166.5 mW, respectively. The heat transfer due to convection can be found from

$$\dot{Q}_{cv} = h A_{cv} |\Delta T|_{cv} \tag{4}$$

where h, A_{cv} and $|\Delta T|_{cv}$ are the convection heat transfer coefficient, surface area of the material and temperature difference between the material and the ambient air, respectively. Convection heat transfer in the single-stage devices is mainly from energy lost from the hot and cold side thermal guards under free convection conditions. Estimates for the h values have been made using the results presented by Haberman and John [6] for horizontal plates and free convection. The h values and $|\Delta T|_{cv}$ are 8.76 W/m^{2}K and 12.5 K for the hot side guard and 4.50 W/m^{2}K and 10 K for the cold side guard, respectively. Based on these values the convective heat transfer for the hot and cold thermal guards are 25.6 mW and 10.5 mW, respectively. The heat transfer due to radiation is

$$\dot{Q}_r = \varepsilon A_r \sigma \left(T_H^4 - T_S^4 \right) \tag{5}$$

where ε, A_r, σ, T_H and T_S are the material's emissivity, surface area, Stefan-Boltzmann constant, hot surface temperature and ambient temperature, respectively. Radiative heat transfer in the single-stage devices is mainly from energy lost from the hot side thermal guard. Based on the silicon emissivity of 0.2 from Sze [7], a T_H of 305.5 K and T_S of 293 K the radiative heat transfer is 6.2 mW.

From these estimates the $\dot{Q}_T$ is 398.3 mW for this experimental case. This is about 2.2 times lower than is expected from the measured 890 mW power supplied to the heater; however, these estimates are based on measured temperatures from various locations on the device. The uncertainty in the temperature measurements of about 1 to 2 degrees is enough to account for this discrepancy. Additional measurements of device component temperatures using more sophisticated equipment and techniques is

necessary to resolve these small heat transfer amounts. In addition, a more accurate determination of effects from the surrounding room air conditions (i.e. free convection or slightly forced convection due to the room's air conditioning) could have resulted in better estimates. The estimates made for the heat transfer are therefore assumed to be approximately the power input to the device heater.

Active Cooling Experiments

The single stage device's cold thermal guard is not actively cooled. This simplistic feature results in the cold side thermal guard warming to a temperature higher than ambient but lower than the hot side due to heat transfer between the two sides. Under most conditions this heat transfer results in a temperature gradient (ΔT) across the aerogel of only about 2 K. An interesting experiment is to consider active cooling of the cold thermal guard during operation by directing a stream of room temperature (~ 293 K) air at the cold thermal guard. Several $(\Delta p_I)_T$ curves have been obtained using this forced convection approach to investigate the effect that active cooling has on device performance. The results for the μKn2 device when using helium and nitrogen for the uncooled (i.e. normal operation) and actively cooled (i.e. with air stream cooling) are shown in Fig. 12. The flow rate of air, which was measured using an in-line flowmeter, was about 0.73 cfm (0.34 L/s). The $(\Delta p_I)_T$ measurements at any given heater power for the actively cooled device resulted in a larger ΔT in comparison to the normal operation. At the higher heater input powers the ΔT across the actively cooled device was measured to be about 2 to 3 K more than the uncooled measurements. Based on the helium $(\Delta p_I)_T$ values and Eq. (1) estimates of the ΔT across the aerogel membrane responsible for the thermal transpiration pressure difference can be found. These estimates are a more accurate measure of the thermal gradient that exists across the aerogel membrane since measuring the temperatures directly during operation in this design is not possible. For the highest power $(\Delta p_I)_T$ values in Fig. 12 for helium the ΔT values have been estimated for both the uncooled (1.71 W) and actively cooled (0.75 W) cases. The measured and estimated ΔT values for the uncooled helium are 4.5 K and 10.58 K, respectively. The measured and estimated ΔT values for the actively cooled helium are 6.5 K and 12.9 K, respectively. From these results it is quite obvious that heat transfer dominates the performance of this device. Minimizing the heat transfer from the hot thermal guard in order to increase the ΔT across the aerogel is paramount for efficient thermal transpiration.

Constant Heater Power Experiments

In order to investigate the effect varying the *Kn* has for the same gas and temperature gradient the power (i.e. voltage) to the heater was kept constant. Each device was set to a constant voltage, which maintained a consistent and steady thermal gradient across each device, and then the pressure was varied in order to study the *Kn* effect. The μKn1 device was set to 22.5 V and this corresponded to a measured ΔT of 1 K at an average temperature of about 312 K and a heater input power of 0.987 W. The μKn2 device was set to 14.5 V and this corresponded to a measured ΔT of 2 K at an average temperature of about 304 K and a heater input power of 0.875 W. Figure 13 outlines the results for the μKn2 device when varying the inlet pressure under constant heater power conditions.

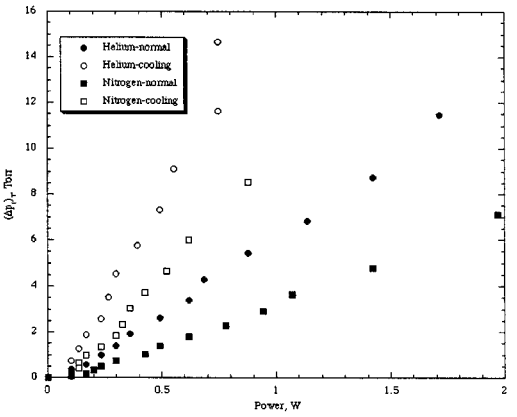

Figure 12: The performance effects from active cooling of the μKn2's cold side thermal guard.

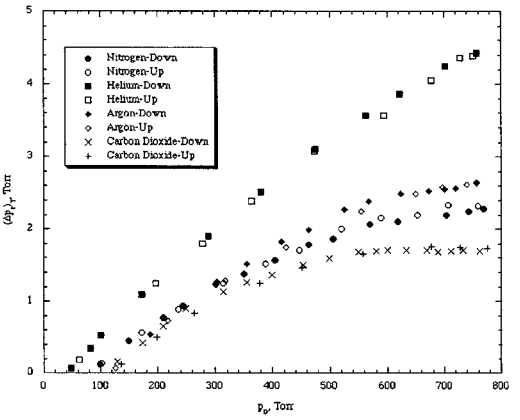

Figure 13: Constant heater power results for μKn2 and varying inlet pressure.

It is interesting to note that μKn2 has greater overall $(\Delta p_I)_T$ values than does μKn1 but both appear to lose efficiency as the inlet pressure approaches atmospheric pressure. Helium remains linear for the entire pressure range but the other gases result in a performance loss at the higher pressures. The lowest pressures for each curve are a result of the inability to measure the very small pressure differentials that exist at these pressures with the differential Baratron transducer.

Throughput Experiments

The throughput, which is the instantaneous fractional pressure change per unit time, has been obtained for both single stage devices at a system pressure of about 760 Torr. These measurements are determined by noting the pressure increase in the differential pressure transducers as a function of time. The measurement run is

completed when the $(\Delta p_I)_T$ value is reached. Each run corresponded to a constant heater power input (set by the voltage) to ensure that the temperature remained steady during the measurements. The μKn1 device was tested using 27.5 V (1.45 W) and 32.5 V (2.07 W). The μKn2 device was tested using 17.5 V (1.15 W) and 20.5 V (1.89 W). Several working gases were used in order to investigate the effect the gas has on the measured throughputs. Representative throughput curves for the lower voltage case for the μKn1 and μKn2 devices are shown in Figs. 14 and 15, respectively. From these two figures it is clear that the μKn2 device pumps gas faster than does the μKn1 device. Based on Fig. 15 the μKn2 device reached $(\Delta p_I)_T$ values in roughly 100 s but the μKn1 device required an average of 200 s. Each device provided various throughput curves depending on the input power and working gas used. Note that the nitrogen curves are slower due to slower thermal speed of nitrogen molecules in comparison to helium.

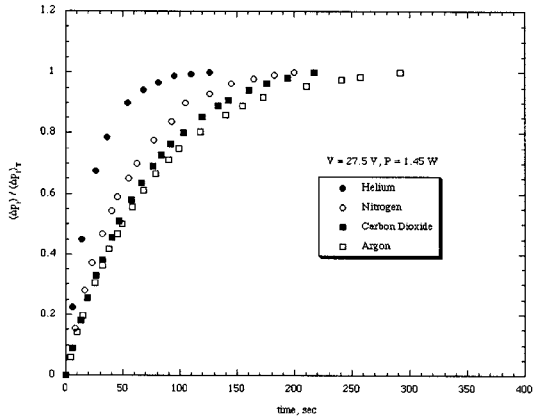

Figure 14: Throughput curves for μKn1 using a 27.5 V heater voltage.

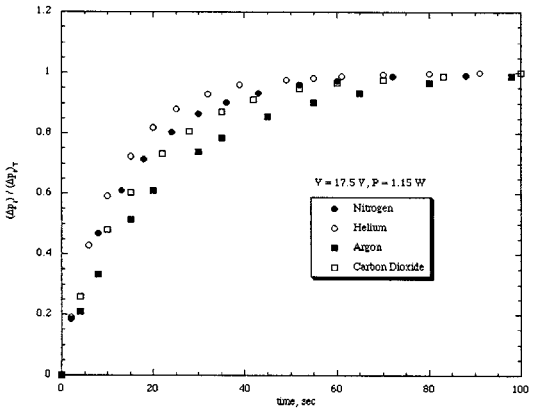

Figure 15: Throughput curves for μKn2 using a 17.5 V heater voltage.

CONCLUSIONS

Future missions and portable applications that utilize vacuum pumped instruments will most likely require novel and integrated MEMS based vacuum pumps. Many conventional vacuum pumps are incapable of being simply scaled down due to complex moving components and a dependence on working fluids and lubricants. The few miniature vacuum pumps that have been developed are not able to meet the demanding mass, volume power and performance requirements of instrument designers. The MEMS Knudsen Compressor is an attractive roughing pump for these types of applications since it has no moving parts and no dependence on fluids or lubricants. From the results presented in the previous section it is clear that the new materials and fabrication methods have resulted in a functional MEMS single stage Knudsen Compressor. The $(\Delta p_I)_T$ and throughput for each device have shown that device assembly is a critical component of building thermal transpiration devices at the microscale. Example calculations for this vacuum pump resulted in a pump of low energy use, small volume and mass. The successful experimental testing of the single stage MEMS devices has provided insight and feasibility for the design and construction of microscale vacuum pumps based on thermal transpiration.

ACKNOWLEDGMENTS

The research described in the paper was performed jointly by the Center for Space Microelectronics Technology, Jet Propulsion Laboratory, California Institute of Technology and the University of Southern California. It was sponsored by the National Aeronautics and Space Administration, Office of Space Science.

Reference herein to any specific commercial product, process, or service by trade name, trademark, manufacturer, or otherwise, does not constitute or imply its endorsement by the United States Government or the Jet Propulsion Laboratory, California Institute of Technology.

REFERENCES

[1] Vargo, S. E., 2000, "The Development of the MEMS Knudsen Compressor as a Low Power Vacuum Pump for Portable and In Situ Instruments," Ph.D. thesis, Univ. of Southern California.

[2] Vargo, S. E. and Muntz, E. P., 1996, "A Simple Micromechanical Compressor and Vacuum Pump for Flow Control and Other Distributed Applications," *American Institute of Aeronautics and Astronautics, 34th Aerospace Sciences Conf.*, AIAA-96-0310, Reno, NV.

[3] Vargo, S. E. and Muntz, E. P., 1996, "An Evaluation of a Multiple-Stage Micromechanical Knudsen Compressor and Vacuum Pump," 20th International Symposium on Rarefied Gas Dynamics, C. Shen, ed., Peking University Press, Beijing, China, pp. 995-1000.

[4] Silica Aerogels - Thermal Properties, 1999, website http://eande.lbl.gov/ECS/Aerogels/satcond.htm/, last updated May 5, 1999.

[5] Hua, D. W., Anderson, J., Di Gregorio, J., Smith, D. M. and Beaucage, G., 1995, "Structural Analysis of Silica Aerogels," J. Non-Crystalline Solids, **186**, pp. 142-148.

[6] Haberman, W. L. and John, J. E. A., 1989, *Engineering Thermodynamics with Heat Transfer*, Allyn and Bacon, Boston, MA.

[7] Sze, S. M. ed., 1994, *Semiconductor Sensors*, John Wiley & Sons, Inc., New York.